Journal of Power Sources 196 (2011) 9276–9283

Contents lists available at ScienceDirect

Journal of Power Sources

journal homepage: www.elsevier.com/locate/jpowsour

Electrochemical performance of nanostructured $La_{0.6}Sr_{0.4}CoO_{3-\delta}$ and $Sm_{0.5}Sr_{0.5}CoO_{3-\delta}$ cathodes for IT-SOFCs

L.M. Acuña [a], J. Peña-Martínez [b], D. Marrero-López [b], R.O. Fuentes [a], P. Nuñez [b], D.G. Lamas [a,c,*]

[a] CINSO (Centro de Investigaciones en Sólidos), CITEFA-CONICET, J.B. de La Salle 4397, (1603) Villa Martelli, Pcia. de Buenos Aires, Argentina
[b] Departamento de Química Inorgánica, Universidad de La Laguna, (E-38200) La Laguna, Tenerife, Spain
[c] Laboratorio de Caracterización de Materiales, Facultad de Ingeniería, Universidad Nacional del Comahue, Buenos Aires 1400, (8300) Neuquén, Pcia. de Neuquén, Argentina

ARTICLE INFO

Article history:
Received 20 June 2011
Received in revised form 19 July 2011
Accepted 20 July 2011
Available online 27 July 2011

Keywords:
Nanocrystalline materials
Intermediate-temperature solid-oxide fuel cells
Cathode
Mixed ionic-electronic conductor
Cobaltite

ABSTRACT

The electrochemical performance of nanostructured cathodes for IT-SOFCs based on perovskite-type mixed ionic/electronic conductors (MIECs) is investigated. Different compounds ($La_{0.6}Sr_{0.4}CoO_{3-\delta}$ and $Sm_{0.5}Sr_{0.5}CoO_{3-\delta}$) and synthesis methods (freeze-drying and citrate complexation) were evaluated. These materials exhibited excellent performance (area-specific resistance values in the range of 0.05–0.20 $\Omega\,cm^2$ for an operating temperature of 700 °C), which improved with decreasing grain size. This performance can be attributed to the high specific surface area of these nanostructured cathodes, thus dramatically increasing the number of active sites for the oxygen reduction reaction. Under these conditions, the electrochemical properties are mainly controlled by oxide ion diffusion through the MIEC cathode, which becomes faster with decreasing grain size.

1. Introduction

Nanostructured materials attract great interest due to their novel properties. They have already been used in power generation and storage devices, such as lithium-ion batteries, low-temperature fuel cells, among others [1]. These materials have limited applications in Solid-Oxide Fuel Cells (SOFCs) because grain growth is expected to occur at the typical operation temperatures of these devices. Nevertheless, their use in intermediate-temperature SOFCs (IT-SOFCs) is currently under investigation because grain growth is reduced by operating in this temperature range. Cathodes based on nanostructured mixed ionic/electronic conductors (MIECs) are particularly interesting because the number of active sites for the oxygen reduction reaction (ORR) is expected to increase dramatically due to the increase in the specific surface area [2–6].

Recent works showed that nanostructured cathodes prepared from $La_{0.6}Sr_{0.4}CoO_{3-\delta}$ nanotubes exhibit low polarization resistances at intermediate temperatures [2,6]. Initially, their enhanced performance was mainly attributed to their high surface-to-volume ratio, increasing the number of reaction sites with the surrounding gas, when compared to an ordinary microstructured cathode [2]. However, a subsequent study showed that oxide ion diffusion enhances with decreasing particle size [6]. This result is similar to the improvement of ionic transport previously reported in nanostructured CeO_2-based electrolytes [7]. Therefore, further investigation is essential to elucidate the electrochemical processes behind the enhanced electrochemical performance of nanostructured MIEC cathodes. In this sense, the study of other compositions and/or nanostructures could be very important. The $Sm_{0.5}Sr_{0.5}CoO_{3-\delta}$ perovskite deserves particular attention because it is considered as a serious candidate for IT-SOFC cathode due to its high performance for the ORR [8–11].

In this work, we evaluated nanostructured $La_{0.6}Sr_{0.4}CoO_{3-\delta}$ (LSC) and $Sm_{0.5}Sr_{0.5}CoO_{3-\delta}$ (SSC) cathodes prepared from nanopowders synthesized by two different wet-chemical methods: freeze-drying and citrate complexation. They were used to prepare pastes with an organic vehicle and deposited on Gd_2O_3-doped CeO_2 (GDC) electrolytes. To retain the original nanostructures in the final cathodes, we use a conventional sintering process at moderate temperatures. The area-specific resistance (ASR) was evaluated using electrochemical impedance spectroscopy (EIS) on symmetrical [cathode/electrolyte/cathode] cells, measured in air. These nanostructured cathodes exhibit very high performance, which is enhanced significantly with decreasing grain size, as in the case of the above-mentioned studies on cathodes based on LSC nanotubes. Their electrocatalytic properties for the ORR are discussed in detail.

* Corresponding author at: Laboratorio de Caracterización de Materiales, Facultad de Ingeniería, Universidad Nacional del Comahue, Buenos Aires 1400, (8300) Neuquén, Pcia. de Neuquén, Argentina. Tel.: +54 299 4490350; fax: +54 299 4490329.
E-mail address: diego.lamas@fain.uncoma.edu.ar (D.G. Lamas).

0378-7753/$ – see front matter © 2011 Published by Elsevier B.V.
doi:10.1016/j.jpowsour.2011.07.067

Table 1
Phase (space group) and morphological data of LSC and SSC powders synthesized by citrate and freeze-drying (FD) methods and calcined at different temperatures. *d*: average crystallite size determined by Scherrer's equation. D_{SEM}: average grain size determined from SEM observations. S_{BET}: BET specific surface area. D_{BET}: average particle size determined from BET specific surface area (see text).

Powder	Synthesis method/calcination temp.	Space group	*d* (nm)	D_{SEM} (μm)	S_{BET} ($m^2\ g^{-1}$)	D_{BET} (μm)
LSC	Citrate/1100 °C	$R\bar{3}c$	>200	≈1	2.1	0.44
	FD/1100 °C	$R\bar{3}c$	>200	≈0.5	2.1	0.44
	FD/900 °C	$Pm\bar{3}m$	30	≈0.25	6.1	0.16
SSC	Citrate/1100 °C	$I4/mmm$	>200	≈2	0.62	1.4
	FD/1100 °C		150	≈1	1.5	0.61
	FD/900 °C		25	≈0.25	4.0	0.22

2. Experimental procedure

2.1. Synthesis and characterization of LSC and SSC nanopowders

LSC and SSC nanopowders were prepared by freeze-drying and citrate complexation methods, starting from $Sr(NO_3)_2$ (Aldrich, 99%), $La(NO_3)_3{\cdot}6H_2O$ (Aldrich, 99.999%), $Co(NO_3)_2{\cdot}6H_2O$ (Aldrich, 98%) and $Sm(NO_3)_3{\cdot}6H_2O$ (Aldrich, 99.9%). These nitrates were first assessed by thermogravimetric analysis to assure the correct cation composition.

The citrate complexation route was carried out using citric acid (Aldrich, 99%) as the complexing agent [12,13]. Each nitrate compound was dissolved in distilled water separately and then mixed to obtain a nitrate solution with the appropriate stoichiometry. A citric acid solution was added at a ligand/metal ratio ($L\,M^{-1}$) of 2 and left under continuous stirring for 24 h. Afterwards, evaporation at 200 °C yielded a homogeneous gel, which was calcined at 1100 °C for 1 h to eliminate the organic material and to obtain the perovskite phase. Samples obtained using this method will be referred hereafter as LSC-citrate and SSC-citrate.

Using the freeze-drying method [14], a stoichiometric solution was prepared from metal nitrates in distilled water, and an ammonium-EDTA solution was added at a molar ratio $L\,M^{-1} = 0.5$ as a complexing agent. The pH was adjusted to 7 by adding nitric acid. The solutions were flash frozen in liquid nitrogen and then dehydrated in a Heto Lyolab 3000 freeze-dryer. The resulting precursors were treated at 300 °C for 1 h, grounded and finally calcined at 900 °C for 5 h. These materials will be referred hereafter as LSC-FD and SSC-FD.

For structural characterization, X-ray power diffraction (XPD) patterns were collected with a PANalytical X'Pert PRO diffractometer equipped with a primary monochromator (Cu $K\alpha_1$ radiation) and an X'Celerator detector. Scans were recorded in the range of $2\theta = 20–80°$, with steps of 0.03° for 2 h. The average crystallite size (*d*) was calculated using Scherrer's equation [15].

BET-specific surface areas (S_{BET}) were determined using a surface area analyzer (Gemini™ 2365, Micromeritics Instrument) with nitrogen as the adsorptive. Prior to the analysis, all samples were degassed at 250 °C under vacuum for several hours. The average grain size was estimated from these results using the equation $D_{BET} = 6/(S_{BET}\,\rho)$, where ρ is the theoretical (crystallographic) density.

The powder morphology and electrolyte/electrode interfaces were analyzed with scanning electron microscopy (SEM) with a JEOL JSM-6300 microscope.

2.2. Preparation and characterization of LSC and SSC cathodes

The electrocatalytic properties of the LSC and SSC cathodes for the ORR were studied with electrochemical impedance spectroscopy (EIS) using symmetric [cathode/electrolyte/cathode] cells.

Dense GDC pellets of about 1.0 mm thickness and 10 mm diameter, prepared from commercial powders ($Ce_{0.8}Gd_{0.2}O_{1.9}$, Nextech Materials) and sintered at 1400 °C for 5 h, were used as electrolytes. A slurry of the different powders mixed with Decoflux™ as the binder was deposited on each side of the GDC electrolyte, and then sintered at different temperatures in the range of 850–950 °C to determine an optimum sintering temperature that yields both an appropriate electrolyte–electrode adherence and the lowest ASR values. Platinum paste (Metalor™) fired at 800–850 °C for 30 min was used as the current collector.

The impedance spectra of these symmetric cells were measured in static air in the temperature range of 400–700 °C using a frequency response analyzer (Solartron 1260) in the frequency range from 0.02 Hz to 1 MHz with an excitation voltage of 50 mV.

3. Results and discussion

3.1. Crystal structure and morphology of LSC and SSC powders

Table 1 summarizes the space group (phase), the average crystallite size and the results of the morphological analysis for all the as-synthesized LSC and SSC nanopowders.

Single-phase perovskite-type powders were obtained after calcination of LSC-FD and SSC-FD at 900 °C for 5 h and LSC-citrate and SSC-citrate at 1100 °C for 1 h. Figs. 1 and 2 show XPD patterns of LSC and SSC powders, respectively. These figures compare the two synthesis methods studied in this work, i.e., citrate complexation and freeze-drying.

In the case of LSC-citrate powders calcined at 1100 °C, the reflections in Fig. 1 exhibit the typical splitting of a rhombohe-

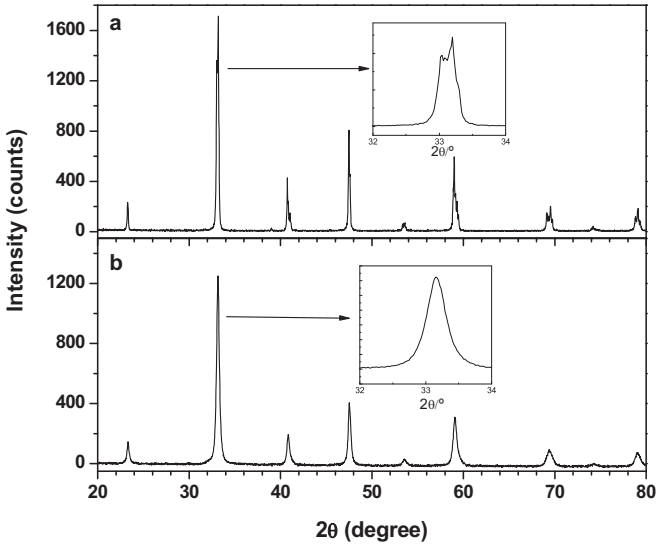

Fig. 1. XPD patterns of LSC powders: (a) synthesized by the citrate complexation method and calcined at 1100 °C and (b) synthesized by the freeze-drying method and calcined at 900 °C. In the former case, all reflections correspond to the rhombohedral phase, while in the latter, they are ascribed to the cubic phase.

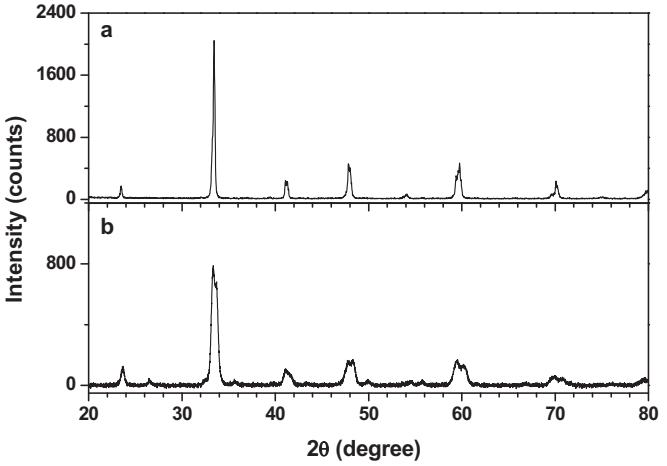

Fig. 2. XPD patterns of SSC powders: (a) synthesized by the citrate complexation method and calcined at 1100 °C and (b) synthesized by the freeze-drying method and calcined at 900 °C. In both cases, all reflections correspond to the tetragonal phase.

dral perovskite-type phase ($R\bar{3}c$ space group), as expected for this composition according to the literature [16]. A similar pattern was obtained for the LSC-FD powders calcined at the same temperature (not shown). Conversely, only the reflections ascribable to the cubic phase ($Pm\bar{3}m$ space group) were found in the case of LSC-FD powders calcined at 900 °C (see Fig. 1). This may be attributed to the small crystallite size of this sample that stabilizes the high-temperature cubic phase at room temperature due to the influence of the surface free energy. It is worthwhile to mention that although citrate and freeze-drying methods yield powders with different phases at room temperature, both materials are expected to have a cubic phase in the temperature range of 500–700 °C because the rhombohedral phase transforms to the cubic one at relatively low temperatures [16].

On the other hand, SSC powders exhibited the tetragonal phase ($I4/mmm$). In the case of the citrate complexation method, single-phase materials were achieved at 1100 °C, while it was possible to use a much lower calcination temperature of 900 °C in the case of the freeze-drying method (see Fig. 2).

The XPD patterns displayed in Figs. 1b and 2b for the freeze-drying powders exhibit diffraction peak broadening due to the smaller crystallite size, as a consequence of the lower calcination temperature needed to obtain the single perovskite phase. By means of Scherrer's equation, the average crystallite sizes of powders synthesized by freeze-drying were calculated to be approximately 30 nm.

Figs. 3 and 4 show the morphology of the LSC and SSC powders, respectively. Fig. 3a corresponds to LSC-FD calcined at 900 °C for 5 h. It can be observed that most of the particles were of 150–250 nm size. On the other hand, Fig. 3b shows that the LSC-citrate powder calcined at 1100 °C for 1 h was mainly composed of aggregate particles of approximately 1 μm. This is because of the higher calcination temperature needed to obtain the single-phase materials in the case of the citrate route.

Similar results were obtained in the case of the SSC powders (Fig. 4). Again, the difference is clear between SSC-FD calcined at 900 °C for 5 h (Fig. 4a) and SSC-citrate calcined at 1100 °C for 1 h (Fig. 4b). The former showed submicrometric grains, while the latter exhibited a wider grain size distribution, from submicrometric grains of approximately 1 μm diameter grains. To verify the strong influence of the calcination temperature on the powder morphology, SSC-FD powder was subjected to a short thermal treatment at 1100 °C for 15 min. As it can be observed in Fig. 4c, a strong grain coarsening was found, with grains of approximately 1 μm or even bigger.

The results of BET specific surface areas, presented in Table 1, were in qualitative agreement with SEM observations. Samples synthesized by freeze-drying and calcined at 900 °C exhibited much larger specific surface areas, about 3 times larger than that of samples calcined at 1100 °C. Table 1 summarizes the average particle sizes determined from BET specific surface areas, D_{BET}, and those estimated from SEM images, D_{SEM}. Both particle sizes resulted in good agreement.

3.2. Microstructure of LSC and SSC cathodes

The nano/microstructure of the different cathodes sintered on GDC electrolytes are shown in Figs. 5 and 6. From these figures, the difference is clear between cathodes obtained with the different synthesis routes analyzed in this work. LSC-citrate and SSC-citrate cathodes synthesized using the citrate method exhibit larger particle sizes than those obtained by the freeze-drying method. Because the as-synthesized powders were calcined at 900 or 1100 °C to obtain the single perovskite phase, using moderate sintering temperatures (850–900 °C) prevents grain growth during the sintering process. This result is clearly shown in Fig. 6a and b, where the SSC-FD cathode consists of fine submicrometric particles (Fig. 6b), in contrast to the SSC-citrate cathode, which exhibited grains of approximately 1 μm. These typical grain sizes are similar to those observed in Figs. 3 and 4.

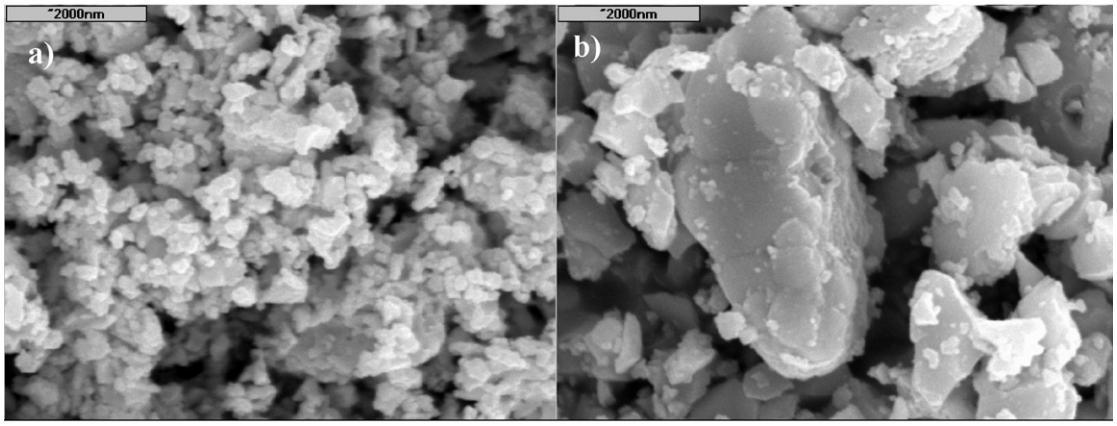

Fig. 3. SEM images of LSC powders: (a) synthesized by the freeze-drying method, calcined at 900 °C for 5 h and (b) synthesized by the citrate complexation method, calcined at 1100 °C for 1 h.

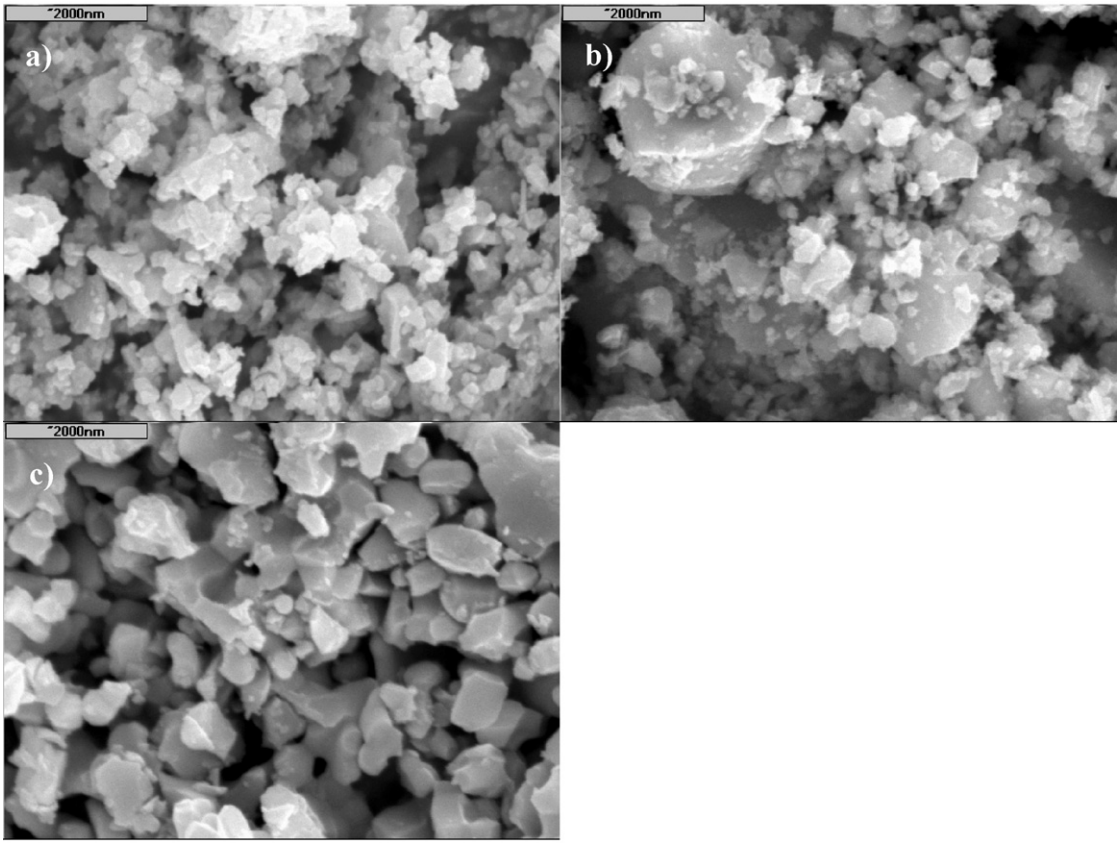

Fig. 4. SEM images of SSC powders: (a) synthesized by the freeze-drying method, calcined at 900 °C for 5 h; (b) synthesized by the citrate complexation method, calcined at 1100 °C for 1 h; and (c) synthesized by the freeze-drying method, calcined at 1100 °C for 15 min.

To study the influence of the synthesis method on the nano/microstructure of the cathodes and on their electrochemical performance, cathodes prepared from LSC-FD and SSC-FD powders calcined at 1100 °C were sintered at 875 °C and 900 °C. Typical SEM micrographs are shown in Figs. 5c and 6c. It can be clearly observed that, in these cases, the grain sizes are smaller than those obtained by the citrate method and bigger than those obtained by the freeze-drying method after calcination at 900 °C. The insets in Fig. 5b and c reflect this feature.

The high porosity of these cathodes is another important aspect to consider because oxygen gas-phase diffusion may play an important role in the electrochemical performance of the cathode. In this way, the resistance due to this process can be minimized, thus enhancing the overall electrochemical performance.

It also can be seen that, at the sintering temperatures of 875–900 °C, very good contact is achieved between cathodes and GDC electrolyte. In these samples, the thickness of the cathodes was approximately 15 μm.

3.3. Electrochemical performance of LSC and SSC cathodes

EIS spectra recorded in the temperature range of 400–700 °C were fitted with different equivalent circuit models. The most reliable model consists of a high frequency (HF) R//CPE in series with a low frequency (LF) Finite Length Warburg (short) element (W_S). The equivalent circuits used for fitting the spectra are shown in Fig. 7d and Fig. 9d. For all the samples, the Warburg element dominated the spectrum. This indicates that the main contribution to the polarization resistance is attributable to oxide ion diffusion through the cathode, as expected for nanocrystalline porous MIECs with a large number of active sites for the ORR. In some cases, a third arc at very low frequencies, which, according to the literature, can be attributed to oxygen gas-phase diffusion [17,18], was detected. As will be discussed below, the best results were obtained for cathodes with thicknesses of approximately 15 μm, prepared by painting three layers of LSC or SSC pastes. Therefore, the results obtained for this thickness will be presented first.

All the impedance spectra have been normalized to the electrode area and divided by two because the symmetrical cell configuration was used for this study. Impedance spectra were shifted to the origin in the Z' axis for easier comparison.

Fig. 7 shows the Nyquist plots obtained for LSC cathodes measured at 700 °C (a typical working temperature in SOFC applications) and the corresponding fitting curves and components. All of the Nyquist plots of LSC cathodes exhibit two main contributions and, in the case of LSC-FD calcined at 900 °C, a third smaller one at lower frequency. Table 2 summarizes the ASR values at 700 °C and the results of the parameters corresponding to the Warburg element obtained by the fitting procedure. The lowest ASR value at 700 °C obtained for LSC cathodes, ASR(700 °C) = 0.084 Ω cm^2, was obtained for cathodes prepared from the LSC-FD powder synthesized at 900 °C. This value is among the best reported in the literature for LSC cathodes [19,20]. It should be noted that the time constant of the Warburg element, W_T, of the LSC-FD cathodes is shorter than that of the LSC-citrate ones. In addition, the W_T of the LSC-FD cathode prepared from the powder calcined at 900 °C is shorter than that corresponding to the cathode prepared from the powder calcined at 1100 °C. Therefore, it can be concluded that the performance of the LSC cathodes improves with decreasing grain size, which is mainly due to the faster oxide ion diffusion (shorter W_T).

Fig. 8a and b shows the Arrhenius plots of LSC cathodes for the ASR and the Warburg resistance (W_R), respectively. As can be observed in Fig. 8a, LSC cathodes prepared from citrate and freeze-

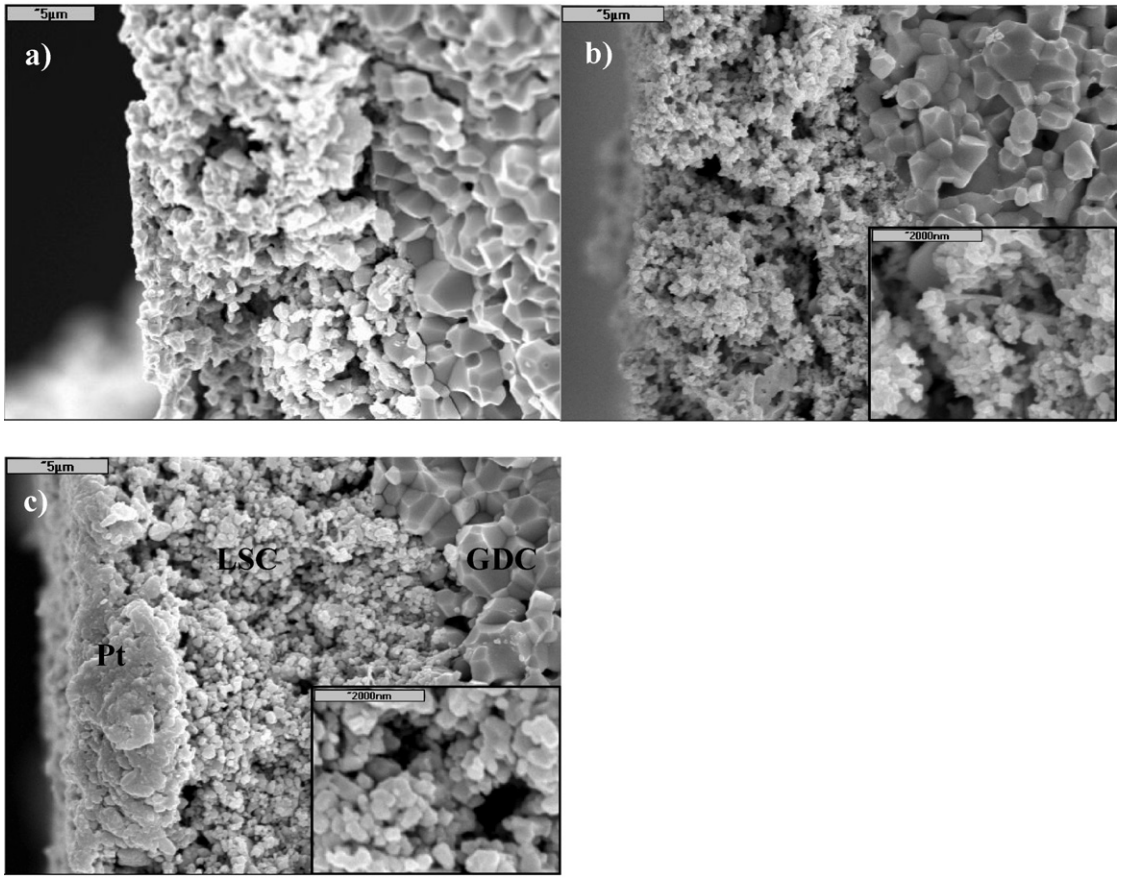

Fig. 5. Cross-section SEM images corresponding to LSC cathodes prepared from the different powders: (a) synthesized by the citrate complexation method, calcined at 1100 °C; (b) synthesized by the freeze-drying method, calcined at 900 °C and (c) synthesized by the freeze-drying method, calcined at 1100 °C. For the sake of comparison, insets show in detail the grains of the cathodes prepared from both LSC-FD powders. All cathodes were sintered on GDC electrolytes at 875 °C. The Pt collector used for electrochemical studies is shown in (c), where it can be observed that the collector did not penetrate into the LSC layer.

drying powders calcined at 1100 °C exhibit a marked change in the slope at temperatures of approximately 450 and 380 °C, respectively, while no changes are detected in the cathodes prepared from freeze-drying powders calcined at 900 °C. These results are in agreement with Petrov et al. [16] and can be interpreted in view of our XPD study at room temperature: LSC powders synthesized by both routes calcined at 1100 °C exhibit the rhombohedral phase such that the rhombohedral-cubic phase transition is expected to occur for increasing temperature, while the freeze-drying powder calcined at 900 °C exhibits the cubic phase and therefore no phase transition takes place. The difference in the transition temperature between both LSC cathodes prepared from powders calcined at 1100 °C is probably due to a difference in the average crystallite size (a higher transition temperature is expected for cathodes with larger average crystallite size).

As far as we know, this is the first time that the retention of the cubic phase of LSC in metastable form at room temperature for small average crystallite sizes (∼ 30 nm) is reported. For instance, Heel et al. reported the synthesis of nanopowders with an average crystallite size of 26 nm that exhibit the rhombohedral phase [21]. These authors reported an ASR value of 0.14 Ω cm^2 at 700 °C for screen-printed cathodes on GDC electrolytes.

It is notable that the activation energy was greater for the cathodes with larger average grain sizes (see Fig. 8 and Table 2). Activation energies, E_a, in Table 2 correspond to the 500–700 °C temperature range.

Fig. 9 shows that the Nyquist plots, measured for SSC cathodes, are also mainly dominated by one arc associated with oxide ion diffusion. Again, the Finite Length Warburg element fitted satisfactorily to the experimental curves. In the case of the SSC-FD cathodes prepared from the powder calcined at 900 °C, the Warburg resistance was small enough [ASR(700 °C) = 0.028 Ω cm^2] to separate the high- and low-frequency arcs. Table 3 summarizes some of the relevant information obtained for SSC cathodes, while Fig. 10 displays the Arrhenius plots and activation energies. As can

Table 2
Relationship between structural data of LSC powders and electrical properties for 15 μm thick cathodes sintered at 875 °C. W_R and W_T are the resistance and the time constant of the Warburg element, respectively. This element dominates the impedance spectra in all cases. T = 700 °C was chosen as a typical operating temperature. E_a: activation energy.

Synthesis method/calcination temp.	ASR (700 °C)(Ω cm^2)	W_R (700 °C)(Ω cm^2)	W_T (700 °C)(×10^{-3} s)	E_a (ASR)(eV)	E_a (W_R)(eV)
Citrate/1100 °C	0.154	0.117	7.7	1.23	1.30
FD/1100 °C	0.170	0.137	4.0	1.30	1.17
FD/900 °C	0.084	0.061	2.1	1.03	1.13

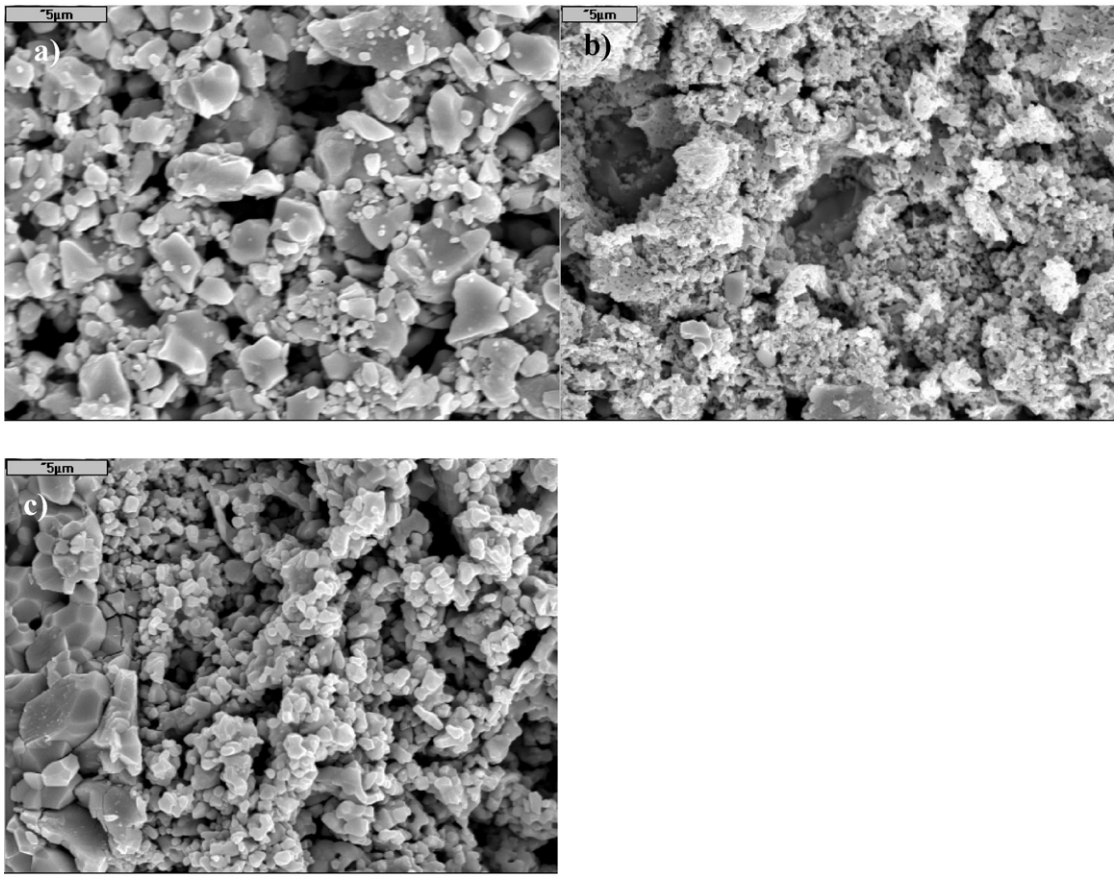

Fig. 6. Surface SEM images corresponding to SSC cathodes: (a) synthesized by the citrate complexation method, calcined at 1100 °C and (b) synthesized by the freeze-drying method, calcined at 900 °C. (c) Cross-section SEM image of SSC-FD cathode calcined at 1100 °C. All cathodes were sintered on GDC electrolyte at 900 °C.

Table 3
Relationship between the structural data of the SSC powders and electrical properties for 15 μm thick cathodes. Cathodes prepared from the powders synthesized by the citrate method calcined at 1100 °C were sintered at 850 °C, while freeze-drying cathodes were sintered at 900 °C. Note that W_R = ASR in the case of cathodes based on powders calcined at 1100 °C.

Synthesis method/calcination temp.	ASR (700 °C)(Ω cm^2)	W_R (700 °C)(Ω cm^2)	W_T (700 °C)($\times 10^{-3}$ s)	E_a (ASR)(eV)	E_a (W_R)(eV)
Citrate/1100 °C	0.110	0.055	18.9	1.07	0.97
FD/1100 °C	0.060	0.043	21.6	0.99	0.96
FD/900 °C	0.049	0.028	4.5	0.88	0.97

be observed, the lowest ASR value was obtained for the SSC-FD cathode sintered at 900 °C [ASR(700 °C) = 0.049 Ω cm^2]. Again, this performance is excellent, among the best reported in the literature for this compound [22–25]. From Table 3, it is clear that the ASR improves with decreasing average grain size. As in the case of LSC cathodes, W_T and E_a decrease with decreasing average grain size, showing that the enhancement of the electrochemical properties of SSC-FD powders calcined at 900 °C is due to faster oxide ion diffusivity.

The influence of the crystallite size on ionic transport was also studied by analyzing the W_T parameter on samples sintered at different temperatures. Fig. 11 shows the dependence of W_T as a function of sintering temperature for samples prepared from powders with different average grain sizes. Again, it is evident that the oxide ion diffusion is faster for cathodes with smaller average grain sizes.

The influence of the thickness of the cathode on its performance was also analyzed. This is an important issue because thin cathodes could have poor performance due to a lower number of active points for the ORR (considering the fast oxide ion diffusion of these materials), while very thick cathodes may have a higher resistance due to oxygen gas-phase diffusion. In all cases, we found an optimum thickness of approximately 15 μm (3 layers). For thicker or thinner thicknesses, the total ASR value at 700 °C increases. For

Table 4
Influence of thickness on the electrochemical properties of the LSC-FD cathodes. All cathodes were calcined at 900 °C and sintered at 875 °C.

Thickness	ASR (700 °C)(Ω cm^2)	W_R (700 °C)(Ω cm^2)	W_T (700 °C)($\times 10^{-3}$ s)	E_a (ASR)(eV)	E_a (W_R)(eV)
7 μm (1 layer)	0.211	0.095	1.7	1.04	1.09
15 μm (3 layers)	0.084	0.061	2.1	1.03	1.13
40 μm (6 layers)	0.097	0.035	1.2	1.01	1.25

Table 5
Influence of thickness on the electrochemical properties of the SSC-FD cathodes. Both cathodes were calcined and sintered at 900 °C.

Thickness	ASR (700 °C)(Ω cm^2)	W_R (700 °C)(Ω cm^2)	W_T (700 °C)(×10^{-3} s)	E_a (ASR)(eV)	E_a (W_R)(eV)
7 μm (1 layer)	0.093	0.033	3.0	0.90	1.01
15 μm (3 layers)	0.049	0.028	4.5	0.88	0.97

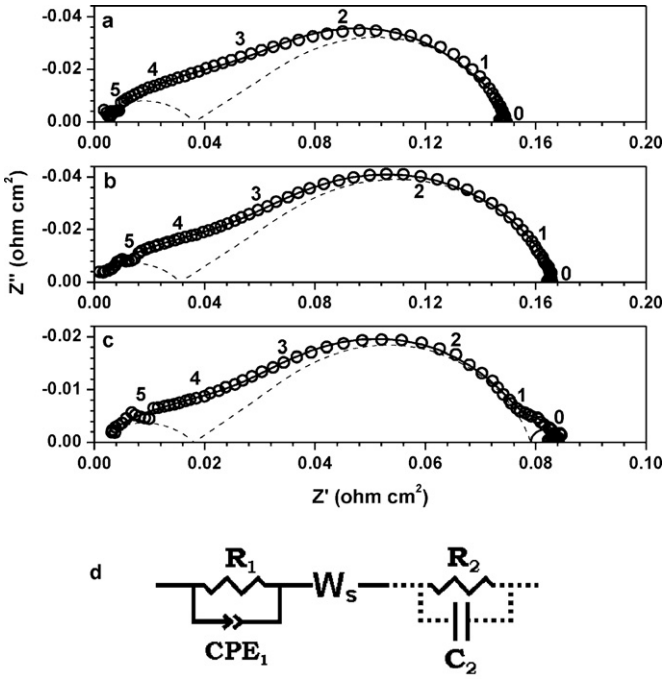

Fig. 7. Normalized Nyquist plots of [LSC/GDC/LSC] symmetric cells, measured at 700 °C (open circles) and fitting curves (solid lines) of (a) the citrate complexation method, calcined at 1100 °C; (b) the freeze-drying method, calcined at 1100 °C; and (c) the freeze-drying method, calcined at 900 °C (note the change in scale of Z' and Z'' axis). (d) Equivalent circuit. Elements connected with dotted lines simulate the low frequency arc in (c). All cathodes were sintered at 875 °C. For easier comparison, impedance spectra were shifted to the origin in the Z' axis. Numbers in the graphics indicate the logarithm of frequency.

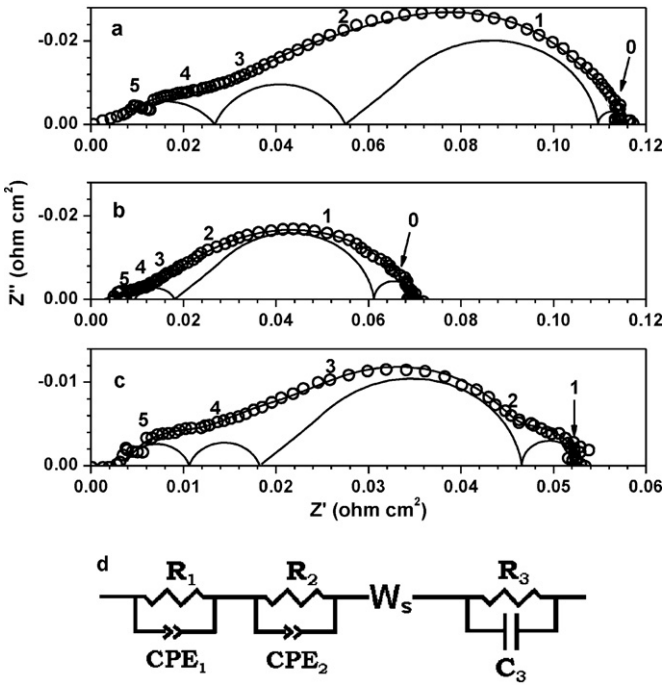

Fig. 9. Normalized Nyquist plots of [SSC/GDC/SSC] symmetric cells, measured at 700 °C (open circles) and fitting curves (solid lines) of (a) the citrate complexation method, calcined at 1100 °C and sintered at 850 °C; (b) the freeze-drying method, calcined at 1100 °C and sintered at 900 °C; and (c) the freeze-drying method, calcined and sintered at 900 °C (note the change in scale of Z' and Z'' axis). (d) Equivalent circuit. Numbers in the graphics indicate the logarithm of frequency.

example, Tables 4 and 5 show our results for cathodes prepared from LSC-FD and SSC-FD nanopowders calcined at 900 °C, demonstrating that cathodes of 3 layers exhibited the best performance. On the other hand, the E_a was almost the same for the different thicknesses, varying in the ranges of 1.01–1.04 and 0.88–0.90 eV for LSC-FD and SSC-FD, respectively.

The stability of nanostructured IT-SOFC cathodes is an important issue for technological applications. A good behavior is to be expected in this case taking into account that the typical operation temperatures are much lower than the sintering temperatures chosen for the preparation of the cathodes. However, our investigation was focused on the electrochemical properties of nanostructured perovskite-type cathodes and therefore we have only tested their

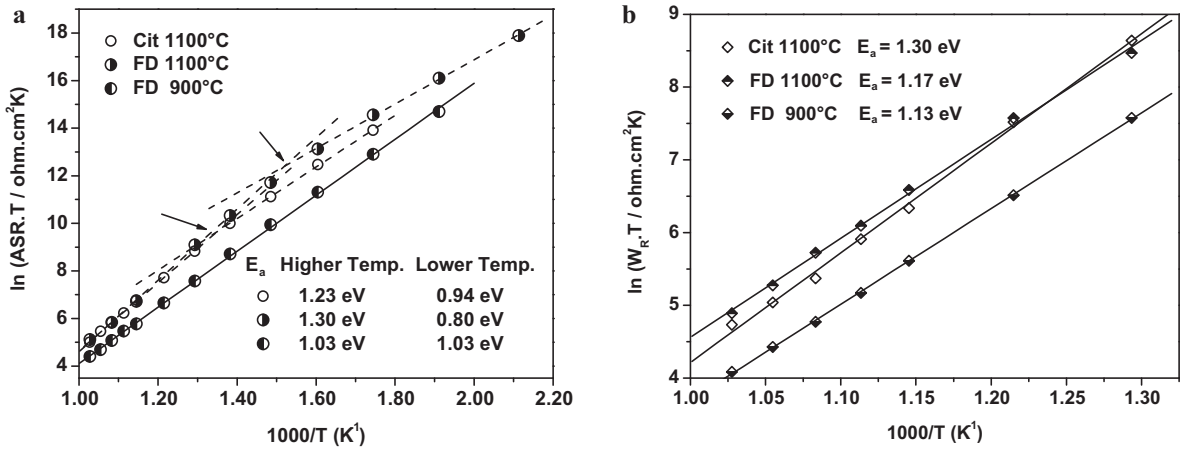

Fig. 8. (a) Arrhenius plots for LSC cathodes. Arrows indicate the change in the slope due to the rhombohedral → cubic phase transition. (b) Arrhenius plots for W_R of LSC cathodes. Activation energies, E_a, are indicated in both cases.

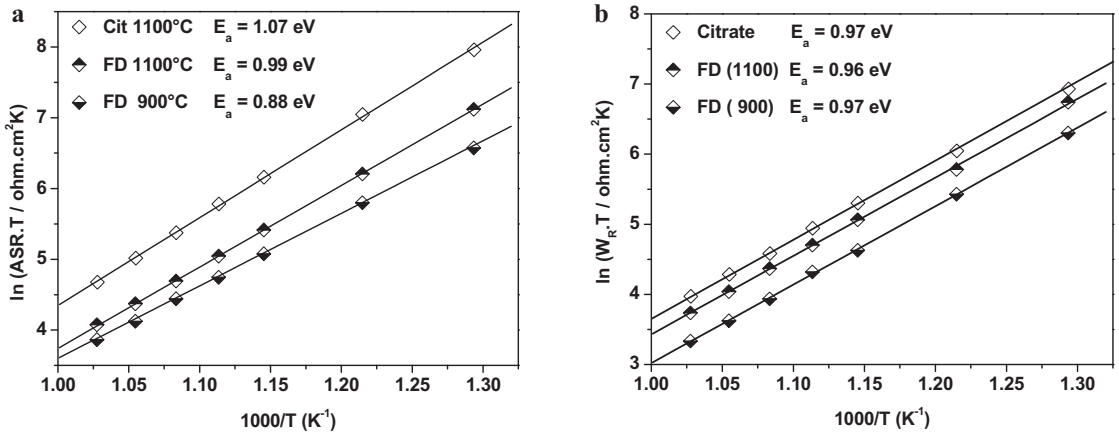

Fig. 10. (a) Arrhenius plots for SSC cathodes. (b) Arrhenius plots for W_R of SSC cathodes. Activation energies, E_a, are indicated in both cases.

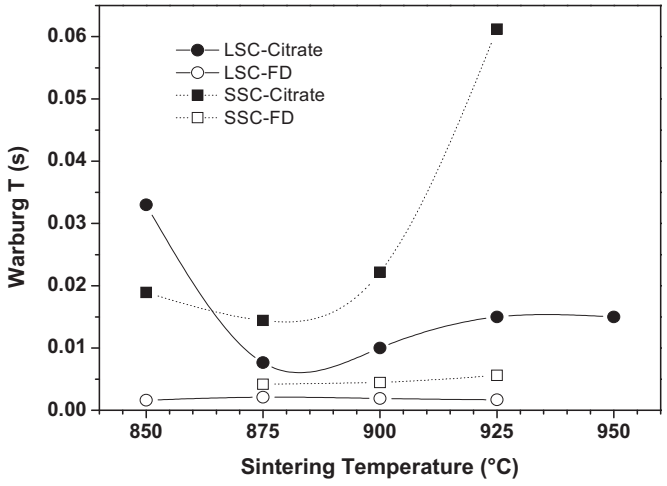

Fig. 11. Influence of the grain size on the oxide ion diffusivity of the cathodes, evaluated in terms of the characteristic time of the Warburg element determined for the LSC and SSC cathodes prepared from powders synthesized by different routes and subjected to different sintering temperatures.

stability during a few hours. Further studies should be conducted to analyze their long-term behavior.

4. Conclusions

In this work, we have presented an electrochemical study of nanostructured LSC and SSC cathodes for IT-SOFCs prepared from nanopowders synthesized by freeze-drying and citrate complexation methods by sintering at moderate temperatures. These materials exhibited excellent performance for the ORR, with ASR values at 700 °C of 0.054 Ω cm^2 for SSC-FD and 0.084 Ω cm^2 for LSC-FD, which are among the smallest values reported in the literature for these compounds.

Our investigation shows that the electrochemical properties of these cathodes is mainly dominated by the oxide ion diffusion process through the cathode, as expected for nanocrystalline porous MIECs with a large number of active sites for the ORR.

In agreement with previous investigations on the properties of cathodes based on LSC nanotubes [6], our EIS study shows that electrochemical performance improves with decreasing grain size, which can be attributed to faster oxide ion diffusivity.

We have also demonstrated that the high-temperature cubic phase can be retained in nanostructured LSC-FD cathodes prepared from nanopowders calcined at 900 °C. In this way, it is possible to avoid the stable rhombohedral phase, which exhibits poor electrocatalytic properties for the ORR.

Acknowledgments

This work was supported by ANPCyT (Argentina, PICT 2005 No. 38309, PICT 2007 No. 01152 and PAE-PICT 2007 No. 02288), CONICET (Argentina, PIP 2005–2006 No. 6559), MICINN (Spain, Mat2007-60127), MAE-AECI (Spain, PCI2007 A/8026/07) and the Canary Islands Government (Spain, PI07/020). R.O. Fuentes and D.G. Lamas are members of CIC-CONICET, Argentina.

References

[1] A.S. Aricò, P. Bruce, B. Scrosati, J.-M. Tarascon, W. Van Schalkwijk, Nat. Mater. 4 (2005) 366–377.
[2] M.G. Bellino, J.G. Sacanell, D.G. Lamas, A.G. Leyva, N.E. Walsöe de Reca, J. Am. Chem. Soc. 129 (2007) 3066–3067.
[3] J. Yoon, R. Araujo, N. Grunbaum, L. Baqué, A. Serquis, A. Caneiro, X. Zhang, H. Wang, Appl. Surf. Sci. 254 (2007) 266–269.
[4] L. Baqué, A. Caneiro, M.S. Moreno, A. Serquis, Electrochem. Commun. 10 (2008) 1905–1908.
[5] J.M. Vohs, R.J. Gorte, Adv. Mater. 21 (2009) 943–956.
[6] J. Sacanell, A.G. Leyva, M.G. Bellino, D.G. Lamas, J. Power Sources 195 (2010) 1786–1792.
[7] M.G. Bellino, D.G. Lamas, N.E. Walsöe de Reca, Adv. Funct. Mater. 16 (2006) 107–113.
[8] T. Ishihara, M. Honda, T. Shibayama, H. Minami, H. Nishiguchi, Y. Takita, J. Electrochem. Soc. 145 (1998) 3177–3183.
[9] T. Hibino, A. Hashimoto, T. Inoue, J. Tokuno, S. Yoshida, M. Sano, Science 288 (2000) 2031–2033.
[10] T. Hibino, A. Hashimoto, M. Yano, M. Suzuki, S. Yoshida, M. Sano, J. Electrochem. Soc. 149 (2002) A133–A136.
[11] C. Xia, W. Rauch, F. Chen, M. Liu, Solid State Ionics 149 (2002) 11–19.
[12] R.O. Fuentes, R.T. Baker, J. Phys. Chem. C 113 (2009) 914–924.
[13] R.O. Fuentes, R.T. Baker, J. Power Sources 186 (2009) 268–277.
[14] D. Marrero-López, J. Canales-Vázquez, J.C. Ruiz-Morales, A. Rodríguez, J.T.S. Irvine, P. Nuñez, Solid State Ionics 176 (2005) 1807–1816.
[15] H. Klug, L. Alexander, X-ray Diffraction Procedures for Polycrystalline and Amorphous Materials, John Wiley, New York, 1974, p. 618.
[16] A.N. Petrov, O.F. Kononchuk, A.V. Andreev, V.A. Cherepanov, P. Kofstad, Solid State Ionics 80 (1995) 189–199.
[17] S.B. Adler, Solid State Ionics 111 (1998) 125–134.
[18] A. Ringuedé, J. Fouletier, Solid State Ionics 139 (2001) 167–177.
[19] P. Hjalmarsson, M. Søgaard, A. Hagen, M. Mogensen, Solid State Ionics 179 (2008) 636–646.
[20] P. Hjalmarsson, M. Søgaard, M. Mogensen, Solid State Ionics 180 (2009) 1395–1405.
[21] A. Heel, P. Holtappels, T. Graule, J. Power Sources 195 (2010) 6709–6718.
[22] S.-W. Baek, J. Bae, Y.-S. Yoo, J. Power Sources 193 (2009) 431–440.
[23] H. Lv, B.-Y. Zhao, Y.-J. Wu, G. Sun, G. Chen, K.-A. Hu, Mater. Res. Bull. 42 (2007) 1999–2012.
[24] I. Park, J. Im, J. Choi, J. Ahn, D. Shin, Solid State Ionics 184 (2011) 35–38.
[25] H. Zhang, F. Zhao, F. Chen, C. Xia, Solid State Ionics 192 (2011) 591–594.